




Enhanced Sub-wavelength Focusing by Double-Sided Lens with Phase Correction in THz Range

M. Rachon¹  · K. Liebert¹ · D. B. But^{2,3} · P. Zagrajek⁴ · A. Siemion¹ · A. Kolodziejczyk¹ · M. Sypek¹ · J. Suszek¹

Received: 8 January 2020 / Accepted: 30 April 2020 / Published online: 13 May 2020
© The Author(s) 2020

Abstract

High capacity radio lines operating in the sub-THz and THz ranges often require very efficient optical elements with a focal length to an aperture diameter ratio—f-number—less than 1. Here, we propose a new type of double-sided sub-THz focusing diffractive optical element with f-number equal to 0.2, designed for quasi-monochromatic illumination with carrier frequency equal to 170 GHz. The element is manufactured by 3D printing technology. Its focal spot diameter defined as the Airy disc size is comparable to the used wavelength. In order to optimize numerically the phase distribution on the anterior side of the structure, we proposed a novel idea based on reversal of phase distribution in outer zones with additional constant phase factor (a method called free form phase distribution, FFPD). Moreover, we applied the modified numerical algorithm to obtain an additional phase correction in a form of a corrective kinoform placed on the posterior side of the diffractive system. The resulted diffractive structure, illuminated by a quasi-plane wave, forms an extremely small focal spot. The paper presents the technical and the theoretical backgrounds, the results of the computer simulations and finally the experimental results.

Keywords Sub-terahertz · Telecommunication · Diffractive lens · Double-sided lens · 3D printing

✉ M. Rachon
rachon@if.pw.edu.pl

¹ Faculty of Physics, Warsaw University of Technology, Warsaw, Poland

² Center for Terahertz Research and Applications (CENTERA), Institute of High Pressure Physics PAS, 01-142 Warsaw, Poland

³ CEZAMAT, Warsaw University of Technology, 02-822 Warsaw, Poland

⁴ Institute of Optoelectronics, Military University of Technology, 2 S. Kaliskiego Str., 00-908 Warsaw, Poland

1 Introduction

The number of applications for sub-THz and THz radiation is constantly growing. It spreads from medical applications and the cancer analysis [1], through telecommunication [2, 3], drugs and explosives detection [4], non-destructive testing during production process (<http://terasense.com/terahertz-technology/terasense/>), to safety measures and agriculture [5]. Due to its non-ionizing character, relatively good spatial resolution and penetration of different media, the THz spectrum of electromagnetic radiation is a constant subject of new research. It is estimated that the size of the THz application market will dynamically grow with each subsequent year (https://www.tematys.fr/reports/en/index.php?controller=attachment&id_attachment=2).

The application of the current work is focused on the telecommunication area. In the case of high capacity (high bit rate) radio lines, it is extremely important to achieve a very efficient concentration of THz radiation on the detector. For the considered wavelengths, the size of the detector is often several dozens of micrometres. Thus, it is necessary to concentrate the incoming radiation into a small spot with a size of the wavelength or smaller. Many methods have been proposed to overcome resolution limit and achieve focal spot with size varying from $\lambda/5$ [6] to even $\lambda/38$ [7].

Generally, one of the three solutions can be used: reflective, refractive or diffractive optics. Focusing the incoming radiation into detector antenna can be obtained by the usage of mirrors [8], which are highly efficient and do not exhibit chromatic aberration. Mirrors are very often used for centimetre waves. However, taking into account the vast field of the THz applications, optical mirrors that are expensive, not compact and difficult to adjust, do not meet all the requirements. The next solution is to use refractive lenses, broadly used in the THz range [9], but to form the sub-wavelength focal spot, their shape should be hyper-hemispherical like [10]. Keeping in mind that the diameter of such lens focusing millimetre waves is typically greater than 5 cm, the thickness of the lens is also of order of centimetres. It results in a significant attenuation in the volume of the lens (in case of polytetrafluoroethylene, PTFE or high-density polyethylene, HDPE) or in an extremely high cost of the less absorbing material (like high resistivity-silicon, HR-Si).

The other approach to overcome the diffraction limit is based on the gradient index micro-lens arrays designed as the metamaterial structure. They can preserve evanescent waves [11] and provide extremely small focal spot. However, the energy transmission of such structures is very low, limiting their practical application. Use of the sophisticated metamaterials and increasing complexity of the structures offers possibility to increase the energy efficiency of such elements [12–14], which still remains low. The other described in literature methods used to overcome the resolution limit relies on micro-lenses arrays [15] or manipulation of source coherence [16]. They enable to improve focusing but exhibit a number of disadvantages like high complexity, low energy efficiency, fragility and high production costs.

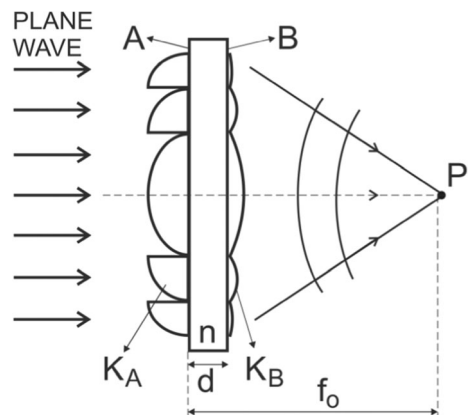
The method proposed in the current paper is based on diffractive optics. Diffractive elements are relatively thin, so they are lighter than refractive ones. Additionally, they require using less material and have lower attenuation in the volume. Moreover, diffractive elements designed for the THz radiation are often relatively cheap in manufacturing (3D printing, injection moulding). However, designing and manufacturing an efficient diffractive structure operating at high diffraction angles creates many challenges as, e.g. suppression of geometrical aberrations and the shadow effect [17].

The aim of this work is to design a diffractive structure effectively focusing THz radiation. A general method based on the use of the phase correcting kinoform was already described [18]. A thorough analysis of the obtained focal spots leads to the conclusion that a volumetric form of the corrective element introduces unwanted aberrations and, therefore, the focusing efficiency is reduced and the focal spot has much larger dimensions—in comparison with its theoretical dimensions (calculated for the diffractive limited structure—Airy disc size). For this reason, this article presents improved methods of the structure design based on the following two modifications. Firstly, the corrective kinoform is designed according to an algorithm that takes into account its volumetric nature and limits its aberrations. Secondly, the modification concerns the improvement of the energy efficiency of the diffraction structure by taking into account the shadow effect. The shadow effect [17] crucially decreases diffraction efficiency in case of large deflection angles. Therefore, the diffractive focusing element with a high numerical aperture (small value of the f-number) has significantly reduced energy efficiency in the outer part, corresponding to the large deflection angles. Such drawback causes additional aberrations reducing quality of focusing. Thus, to suppress this unwanted effect, in this work, the use of the novel diffraction structure called free form phase distribution (FFPD) is proposed. The usefulness of the proposed modifications has been verified by numerical calculations and experiments for systems with a very large numerical aperture, corresponding to the number f-number equal to 0.2.

2 Basic Algorithm

For clarity, we present the general principle of focusing performed by the diffractive structure described in Ref. [18] and illustrated in Fig. 1. The system consists of the following three parts. A flat-parallel substrate of a thickness d with two kinoform elements placed on the anterior side A (K_A) and posterior side B (K_B). The former corresponds to the converging lens, while the latter to the corrective kinoform. A plane wave incident perpendicularly to the substrate is transformed into a spherical wave, converging in the point P, distant by f_0 from the side A. The substrate and both kinoforms are made of material with a refractive index n . Neglecting this refractive index and assuming propagation in air, the THz fields in the planes A and B correspond to the following non-paraxial transmittances of thin lenses [19, 20]:

Fig. 1 The diffractive system focusing incident plane wave into the point P is consisted of a flat-parallel substrate and two kinoforms K_A and K_B



$$T_A(r) = e^{iK_A} = e^{-ik\sqrt{r^2+f_0^2}}, \quad (1)$$

$$T(r) = e^{-ik\sqrt{r^2+f^2}}, \quad (2)$$

where $k = 2\pi/\lambda$, λ is a wavelength of THz radiation, $f = f_0 - d$ and r is the radial coordinate in the polar coordinate system. The function $T_A(r)$ defines the transmittance of kinoform K_A ; however, assuming its volumetric nature and the refractive index of the substrate ($n > 1$), the THz field in the plane B differs from that described by the transmittance $T(r)$. According to the numerical analysis, this field has a negligible variable amplitude and can be defined as the following phase field:

$$T_1(r) = e^{i\varphi_1}, \quad (3)$$

where φ_1 is the phase of radiation after propagation by the kinoform K_A and the substrate. Therefore, to obtain the field described in Eq. 2 behind the kinoform K_B , its transmittance should be expressed as follows:

$$T_B(r) = T_1^*(r)T(r), \quad (4)$$

where the symbol $*$ denotes complex coupling. This algorithm, proposed in Ref. [18], assumes the infinitely thin corrective kinoform K_B . In reality, it is a volumetric structure, introducing a phase shift of up to 2π , with the following maximal relief height:

$$h_{max} = \frac{\lambda}{n-1}. \quad (5)$$

Therefore, kinoform K_B introduces additional aberrations resulting in less effective focusing than assumed. This basic algorithm was verified in Ref. [18] and enabled to increase the radiation intensity in an assumed focal point, but the focal spot size was much larger in comparison to theoretical predictions. For previously described structures [18] with the diameter of 50 mm and a focal length of 50 mm (f-number = 1), designed for 300 GHz, manufactured from polyamide (PA12, by selective laser sintering) with a refractive index $n = 1.64$ and an absorption coefficient $\alpha = 0.27 \text{ cm}^{-1}$ (@ 300 GHz), we observed evident focusing improvement [18]. The intensity peak value in the focal spot was increased almost twice (1.79×). Nevertheless, a diameter of the Airy disc equal to 4.20 mm was substantially enlarged in respect to the diameter 2.44 mm predicted theoretically in the case of the number f-number equal to 1 [21].

In order to avoid aberrations of the corrective kinoform (K_B), its relief should be possibly low, slowly varying and easy to manufacture. In practice, this means the best possible mutual matching of the functions $T_1(r)$ and $T(r)$. To resolve this issue, we propose the algorithm modifications, described in the following two sections.

3 Modified Algorithm

The simplest approach based on the geometric optics and the paraxial approximation leads to the conclusion that the substrate with a thickness of d and a refractive index n increases the focal distance (Fig. 2). If the field behind the kinoform K_A corresponds to a convergent spherical wave with the radius of curvature f_0 , then behind the plane B of the substrate, we get focusing with the enlarged focal length equal to $f + \Delta x$, where $\Delta x = d(n - 1)/n$.

Based on this simple example, it can be assumed that the volumetric nature of both the kinoform K_A and the substrate shift the focal spot further along optical axis—from the expected point P to the point P' (Figs. 2 and 3). In this case, the function $T_B(r)$ defining the corrective kinoform transmittance (Eq. 4) is best matched to the function $T(r)$ when it is defined by the phase of the THz field propagated in air to the plane C located at a distance x behind the plane B. Numerical analysis confirms this assumption. Therefore, the modified algorithm for determining the transmittance of the corrective kinoform K_B is based on the selection of the optimal distance x . As a criterion to determine this distance, we have chosen the maximal intensity in the assumed focal point P. The optimal distance x cannot exceed the theoretical maximal thickness h_{\max} of a relief of the kinoform K_B (Eq. 5). Numerical calculations are made for distances x with values $x_n = h_{\max}m/M$, where M is a sufficiently large natural number and $m = 0, 1, 2, \dots, M$.

4 Free Form Phase Distribution (FFPD) Element

The second proposed modification concerns the kinoform K_A , generating a spherical wave with a radius of curvature f_0 (Fig. 1). The kinoform K_A with a small f-number (less than 1) results in small widths of outer zones which become comparable or smaller than the maximal relief height h_{\max} (Eq. 5). In this case, the shadow effect, described in Ref. [17], starts to play a significant role. Most of the THz radiation incident on the kinoform is redirected in (-1) instead of $(+1)$ order of diffraction. Therefore, the outer part of the kinoform K_A has a very low diffraction efficiency. This introduces additional aberrations, resulting in a substantial difference between the THz field in the plane A and the expected spherical convergent wave

Fig. 2 According to the paraxial approximation ($\alpha \ll 1$ and $\beta \ll 1$) the substrate shifts the convergence point of the incident spherical wave by Δx

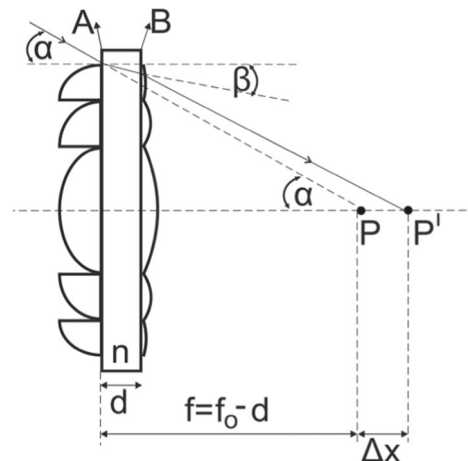
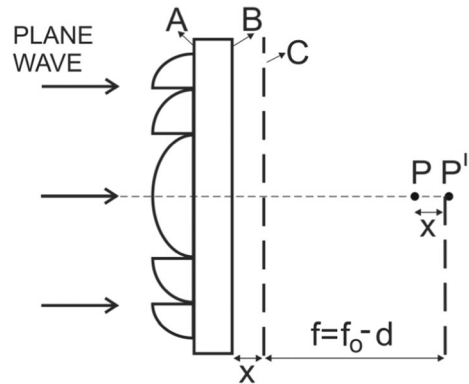


Fig. 3 Transmittance of the corrective kinoform is defined by the THz field in the plane C resulting after propagation by the kinoform K_A , the substrate and a distance x in air



described by (Eq. 1). The proposed modification assumes the design of the kinoform K_A as the free form phase distribution (FFPD) element, patented lately by the authors [22]. A scheme of the FFPD structure is shown in Fig. 4. Its central part is a classic kinoform generating the spherical convergent wave, while the outer part of the structure is designed for the spherical divergent wave with the same radius of curvature f_0 . As a result of the shadow effect, this divergent field is transformed into the expected field converging into the point P (Fig. 1). Both converging waves interfere with each other, and in order to ensure a constructive interference, the outer part contains an additional phase retardation. This phase shift and the optimal dimensions of the central and outer parts are numerically determined in order to get maximal light field intensity in the focal point P, assuming propagation in air behind the plane A (Fig. 1).

5 Numerical Modelling Results

Modelling algorithm was based on wave optics approach and included non-paraxial propagation effects. The propagation was calculated using angular spectrum of plane waves method (ASPW) with additional assumptions like larger calculation matrix to suppress numerical edge effects, propagation kernel not simplified to paraxial approximation and change of the

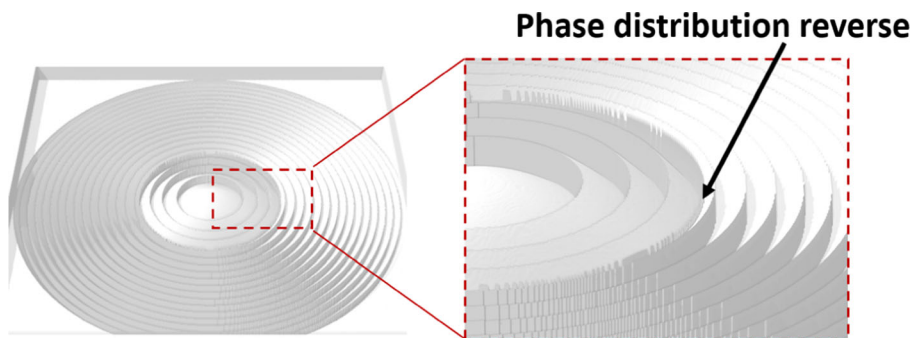


Fig. 4 An illustration of the FFPD principle. The reliefs of different geometry in the central and the outer part of the element are designed for a convergent and a divergent wave, respectively. According to the shadow effect both parts form fragments of a spherical convergent waves with the same curvature radii. The additional substrate in the outer part enables constructive interference of these waves in the assumed focal point

refractive index while propagation through different media. Mostly, introducing any optical elements into the simulated optical setup results in multiplying particular light field distribution with transmittance of this element and takes place in one plane. It is assumed that element introduces particular phase shifts but is ideally flat. In case of real structures, this condition is not fulfilled anymore; thus, we propose using different approach to ASPW method. We assume that introduced phase distribution is not planar but has particular thickness (either calculated from Eq. 5 or being a particular constant thickness in case of substrate). A volume of the entire diffractive structure is divided into thin slices. The propagation of the light field between slices (in the volume of kinoform K_A , substrate and free space) was calculated using the non-paraxial approach of the modified convolution method (MCM, corresponding to ASPW method) [23, 24] including evanescent waves in the kernel. After such process, we obtain amplitude and phase distributions after the real structure (lens or FFPD element) that are different from assumed transmittance of the element. Thus, there is a need to correct it, adding transmittance at plane B. To obtain better results in simulations, we also assumed the existence of the substrate layer, which influenced phase distribution of the corrective kinoform. Then, using the modified algorithm air space behind the plane B was divided into $M = 32$ slices each 0.09 mm thick, in order to find an optimal position of the plane C (Fig. 3). Finally, we have chosen the distance x providing the maximal intensity in the assumed focal point P.

For comparative purposes we performed numerical simulations for the following four diffractive structures, all having the focal length equal to $f_0 = 20$ mm and diameter $D = 100$ mm:

- (1) *Lens* (K_A)—the basic focusing system without the corrective kinoform K_B . It consists of the classical kinoform K_A with the transmittance defined by Eq. 1 and the substrate (Fig. 1).
- (2) *Lens + Correction* (K_A and K_B)—the focusing structure consisting of the classical kinoform K_A with the transmittance defined by Eq. 1, the substrate and the corrective kinoform K_B designed according to the modified algorithm (Fig. 1).
- (3) *FFPD element* (K_{FFPD})—the focusing structure without the corrective kinoform. It consists of the kinoform analogical to K_A with the transmittance defined by Eq. 1, but designed as the FFPD element, with added substrate. It is named K_{FFPD} .
- (4) *FFPD element + Correction* (K_{FFPD} and K_{COR})—the focusing structure consisting of the kinoform K_{FFPD} and the corrective kinoform analogical to K_B designed according to the modified algorithm and named K_{COR} .

The numerical modelling was conducted on a 4096×4096 pixel matrix with sampling of $117 \mu\text{m}$ in both directions. Modelled structures were equivalent to the real ones made by laser sintering from polyamide 12 (PA12) [5]. We have taken into account volumetric nature of the kinoforms K_A , K_B and the substrate (Fig. 1). Pixel size was chosen basing on the available voxel size of the 3D printing machine (SLS process). In this article, the structures were designed for a wavelength equal to $\lambda = 1.76$ mm in air which corresponds to a frequency of 170 GHz. Measured samples of the PA12 have the refractive index $n = 1.59$ and the absorption coefficient $\alpha = 0.25 \text{ cm}^{-1}$ for this frequency. Then, the 2π phase shift realized by the kinoforms corresponds to their maximal thickness equal to $h_{\text{max}} = 2.98$ mm. The assumed structure parameters are as follows: the focal length $f_0 = 20$ mm, the diameter $D = 100$ mm and the thickness of the substrate $d = 1$ mm.

The phase distributions of selected kinoforms of these four structures are illustrated in Fig. 5. In order to evaluate efficiency of focusing, we measured maximal intensity at an assumed focal distance behind the structure. The value of the measured intensity for the basic structure (1) has been normalized to one, and the intensities generated by other structures are presented in reference to it: 2.76, 2.64 and 3.35 for the structures 2, 3 and 4, respectively.

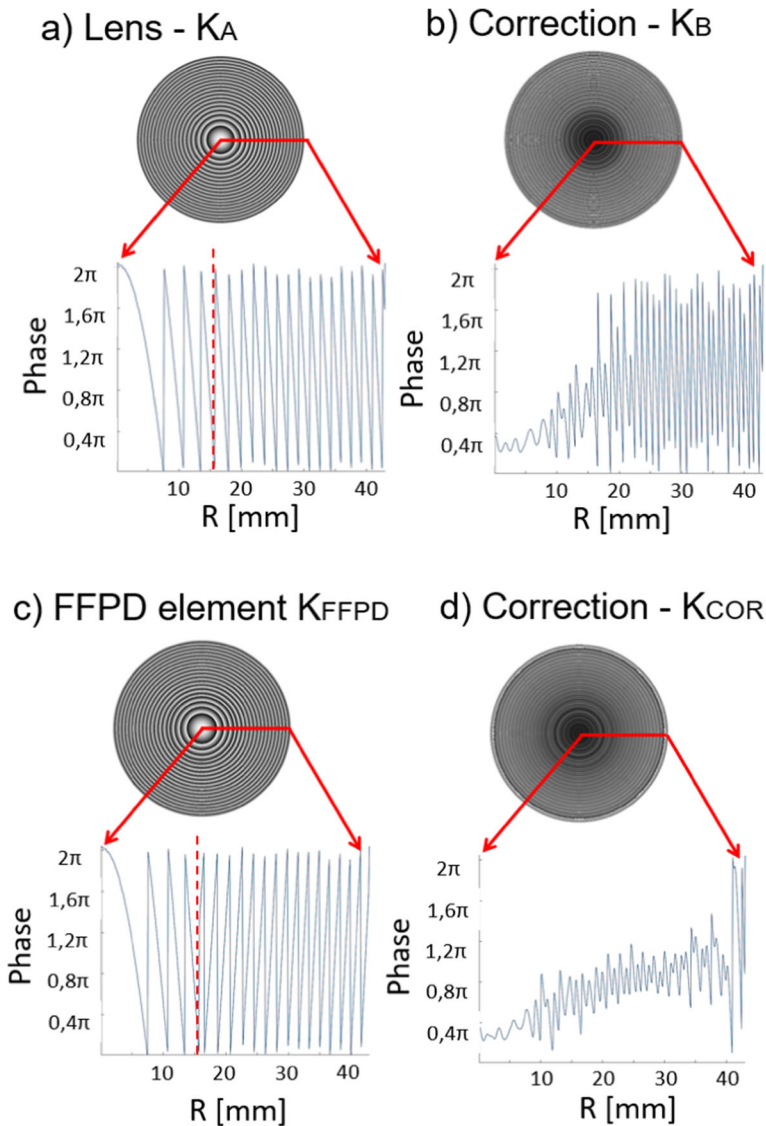


Fig. 5 An illustration of the phase transmittances of **a** kinoform K_A in the basic structure (1), **b** corrective kinoform K_B in the structure (2), **c** kinoform K_{FFPD} in the structure (3) and **d** corrective kinoform K_{COR} in the structure (4). Black colour represents 0π phase shift, while white denotes 2π phase shift. Cross sections illustrate the details of phase distributions of a kinoform where a bottom line represents 0π phase shift and a top line denotes 2π phase shift. Red dashed line indicates the radius dividing the structure to inner and outer zones. In **c** an inverted zones in the outer zones are visible

According to simulation results, corrective kinoforms designed by the modified algorithm substantially enhance focusing efficiency. The structures (2) and (4) increase the maximal intensity 2.76 and 3.35 times, respectively. It is a clearly better result than in a case of application of the basic algorithm described in Ref. [18], when the corrective kinoform improved this intensity only by 1.79 times. The use of the FFPD element as the kinoform on side A considerably modifies structure of the corrective kinoform K_{COR} . Comparing Fig. 5b and d, its relief is lower and more smooth with notably smaller fluctuations. It is an important advantage, because such structure is easier for fabrication which in turn limits possible unwanted aberrations of the corrective kinoform caused by technological imperfections. Moreover, the highest intensity corresponding to the structure (4) suggests that application of the FFPD element suppress aberrations and improves diffraction efficiency of the kinoform on side A.

6 Experimental Results

The experimental setup (illustrated in Fig. 6) consisted of a VDI multiplier as a source with a pinhole for quasi-spherical wave creation. At a distance of 1 m, a semi-plane wavefront was formed. The XY plane was scanned by the single GaAs HEMT detector.

In the experiment, the four described and numerically modelled structures were examined. Diffractive elements were fabricated with selective laser sintering process (SLS) on EOS GmbH machine. This additive manufacturing process sinters material, in this case powdered polyamide PA12, with the use of laser. Voxel size of used 3D printing technique is $39 \mu\text{m} \times 39 \mu\text{m}$ in x- and y-axes. Growth layer thickness in case of HD printing mode is theoretically equal to $30 \mu\text{m}$. The sampling used in modelling was equal to $117 \mu\text{m}$ which corresponded to three voxels of a 3D printer in order to obtain the correct printout and quality. The tolerance of used machine was 0.3%, and theoretical final accuracy was in the 0.05 to 0.1-mm range.

STL models of the kinoforms manufactured from polyamide PA12 with the laser sintering 3D printing method are presented in Fig. 7. Maximal intensity values of focal spots for numerical simulations and experimental results are shown in Fig. 7 (yellow inset in each graph). The maximal intensities corresponding to the structures were referred to the structure

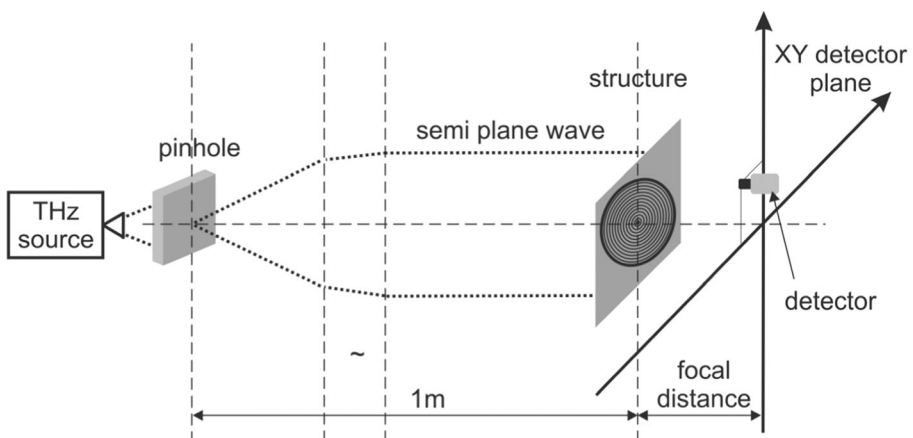


Fig. 6 The scheme of the experimental setup using fast and sensitive GaAs HEMT detectors

(1) with the lowest efficiency, generating the maximal intensity normalized to 1. Figure 7 presents 2D intensity distributions measured experimentally in focal planes of the four analysed focusing structures.

The diffraction limit defined by the Rayleigh criterion [21] is given as follows:

$$l = \frac{1.22DWL}{\sin(\alpha)}, \tag{6}$$

where l is a diameter of the first intensity minimum of the focal spot, α is the maximal angle of deflection realized by the focusing system and DWL denotes a designed wavelength equal to 1.76 mm in our case. Generally, assuming the fixed DWL, dimensions of the focal spot increase with the f-number = f_0/D . Particularly we obtain the following diameters:

$$l = \frac{1.22 \cdot 1.76}{0.93} = 2.3\text{mm} \tag{7}$$

$$l = \frac{1.22 \cdot 1.76}{0.45} = 4.77\text{mm} \tag{8}$$

in case of a f-number equal to 0.2, used in the design of the analysed focusing systems (Eq. 7), and for comparison in case of a f-number equal to 1, corresponding to our previous systems described in Ref. [18] (Eq. 8). White circles in Fig. 7 illustrate diffraction limits, and they have diameters determined by Eqs. 7 and 8.

The biggest difference between numerical modelling and experiment can be observed for the structure (2). This result coincides well with remarks given in the former section. In this

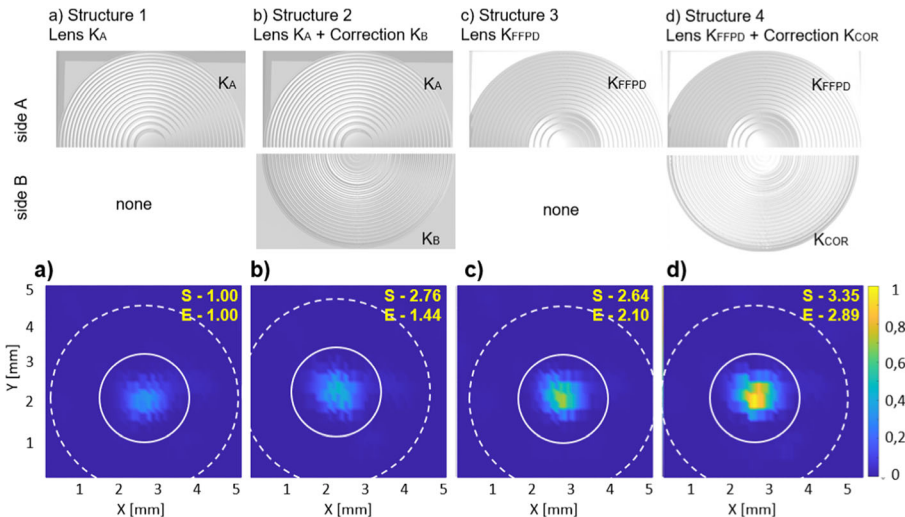


Fig. 7 The photographs of manufactured structures. The comparison of experimental focal spots formed by the following four analysed diffractive structures: **a** structure (1) Lens (K_A), **b** structure (2) Lens + Correction (K_A and K_B), **c** structure (3) FFPD element (K_{FFPD}) and **d** structure (4) FFPD element + Correction (K_{FFPD} and K_{COR}). The white circles illustrate diffraction limits defined by Eq. 7 (solid line) and Eq. 8 (dashed line). Yellow insets in graphs corresponds to the maximal intensity values of focal spots for numerical simulations (S) and experimental (E) results

case, the kinoform K_A suffers the shadow effect inducing aberrations and decreasing diffraction efficiency (Fig. 5a). Then the corrective kinoform has a high relief with strong fluctuations (Fig. 5b) which causes imperfections of the structure during 3D printing process. In turn these imperfections introduce additional aberrations and substantially disturb expected focusing. Moreover, experiments confirm our assumptions that the most efficient focusing provides the structure (4) consisting of the FFPD element and the corrective kinoform designed according to the modified algorithm. The improvement of the maximal intensity ($2.89\times$) is clearly better than in a case of application of the basic algorithm described in [18] ($1.79\times$), and it coincides quite well with the improvement calculated numerically ($3.35\times$).

7 Summary

This work describes a diffraction structure focusing effectively THz radiation and consisting of two kinoforms separated by a substrate in the form of a flat-parallel plate. The general idea of such a structure with additional correction was described in Ref. [18]. To improve focusing, the following two enhancements have been made to the design of the applied kinoforms. The kinoform on the anterior side was designed in a novel form as the free form phase distribution (FFPD) element, limiting the shadow effect and appearing in outer parts of diffractive structures with large numerical apertures. Moreover, the posterior side with a corrective kinoform was designed according to the modified algorithm, taking into account the volumetric nature of the structure.

Frequently, in order to efficiently detect light in the THz range, it is necessary to focus the incident radiation on a detector with sub-wavelength dimensions. Therefore, we have analysed numerically and experimentally the diffractive structures with a very large numerical aperture corresponding to the f-number equal to 0.2, much smaller than that characterized structures described in Ref. [18] (f-number equal to 1). According to the obtained numerical and experimental results, the modifications substantially reduce system aberrations and facilitate the fabrication of the corrective kinoform. Due to larger numerical aperture, it was possible to achieve a much better improvement of radiation intensity in the assumed focus compared with the method described in Ref. [18] – 2.89 and 1.79 times, respectively. According to experimental results shown in Fig. 7, the used of small f-number equal to 0.2 effectively decreases dimensions of focal spots. Radiation intensity captured by the THz detector is located entirely in an area predicted by the diffraction limit defined according to Eq. 6 (white solid line circles in Fig. 7). It is a substantial progress in comparison to results obtained for a greater f-number equal to 1 and diffractive structure based on classic kinoforms and the basic algorithm given in Ref [18]. In previously described case, the measured diameter of the focal spot (4.2 mm) was substantial larger than that predicted by the diffraction limit (2.44 mm). Moreover, according to Fig. 7 radiation intensity within a focal spot depends strictly on design of applied kinoforms. The best focusing provides the structure consisting of a kinoform K_{FFPD} and a corrective kinoform K_{COR} designed by the modified algorithm (Fig. 7d). According to the obtained numerical and experimental results, such a structure enables sub-wavelength effective focusing of THz radiation.

Acknowledgements The authors would like to thank the Ortech Company for providing LS 6.0 Software used for designing and modelling diffractive optical elements in the THz range.

Funding Information This research was supported by Warsaw University of Technology; Foundation for Polish Science Grant Nos. TEAM/2016-3/25; The ‘Center for Terahertz Research and Applications’ (CENTERA—‘International Research Agendas’ programme of the Foundation for Polish Science co-financed by the European Union under the European Regional Development Fund) and by the National Center for Research and Development under the LIDER programs: LIDER/020/319/L-5/13/NCBR/2014 and LIDER/11/0036/L-9/17/NCBR/2018.

Open Access This article is licensed under a Creative Commons Attribution 4.0 International License, which permits use, sharing, adaptation, distribution and reproduction in any medium or format, as long as you give appropriate credit to the original author(s) and the source, provide a link to the Creative Commons licence, and indicate if changes were made. The images or other third party material in this article are included in the article's Creative Commons licence, unless indicated otherwise in a credit line to the material. If material is not included in the article's Creative Commons licence and your intended use is not permitted by statutory regulation or exceeds the permitted use, you will need to obtain permission directly from the copyright holder. To view a copy of this licence, visit <http://creativecommons.org/licenses/by/4.0/>.

References

1. Y. Calvin, F. Shutting, S. Yiwen, E. Pickwell-MacPherson, *Quant Imaging Med Surg* 2, 33 (2012)
2. T. Kleine-Ostmann, T. Nagatsuma, *J Infrared Millim Terahertz Waves* 32, 143 (2011)
3. R. Vilar Mateo, J. Marti Sendra, R. Czarny, M. Sypek, M. Makowski, C. Martel, T. Crepin, F. Boust, R. Joseph, K. Herbertz, T. Bertuch, A. LeFevre, F. Magne, *Microw J (Int Ed)* 57, 28 (2014)
4. P. T. Taday, *Philos, Trans A Math Phys Eng Sci* 362, 351 (2003)
5. J. Suszek, A. Siemion, M. Bieda, N. Blocki, D. Coquillat, G. Cywiński, E. Czerwińska, M. Doch, A. Kowalczyk, N. Palka, A. Sobczyk, P. Zagrajek, M. Zaremba, A. Kolodziejczyk, W. Knap, M. Sypek, *IEEE Trans Terahertz Sci Technol* 5, 314 (2015)
6. A. Grbic, G. V. Eleftheriades, *Phys. Rev. Lett.* 92, 117403 (2004)
7. J. Zhao, W. Chu, L. Guo, Z. Wang, J. Yang, W. Liu, Y. Cheng, Z. Xu, *Sci Rep* 4, 3880 (2014)
8. C. Bruckner, G. Notnia, and A. Tünnermann, *Optik* 121, 113 (2010).
9. J. Richter, A. Hofmann, L.-P. Schmidt, *Proceedings of the 31st European Microwave Conference*, 347 (2001)
10. M. Tonouchi, M. Tani, Z. Wang, K. Sakai, M. Hangyo, N. Wada, Y. Murakami, *IEEE Xplore* 7, 2913 (1997)
11. J. B. Pendry, *Phys. Rev. Lett.* 85, 3966 (2000)
12. H. T. Chen, W. J. Padilla, J. M. O. Zide, A. C. Gossard, A. J. Taylor, R. D. Averitt, *Nature* 444, 597 (2006)
13. M. Byun, D. Lee, M. Kim, Y. Kim, K. Kim, J. G. Ok, J. Rho, H. Lee, *Sci Rep* 7, 46314 (2017)
14. Z. Wang, W. Guo, L. Li, B. Luk'yanchuk, A. Khan, Z. Liu, Z. Chen, M. Hong, *Nat Commun* 2, 218 (2011)
15. K. Allen, N. Farahi, Y. Li, N. I. Limberopoulos, D. E. Walker Jr., A. M. Urbas, V. N. Astratov, *Opt Express* 23, 24484 (2015)
16. C. Liang, G. Wu, F. Wang, W. Li, Y. Cai, S. A. Ponomarenko, *Opt Express* 25, 28352 (2017)
17. J. Suszek, M. Sypek, M. Makowski, F. Garet, I. Ducin, K. Kakarenko, J. Bomba, J.-L. Coutaz, *Opt Lett* 38, 1464 (2013)
18. M. Rachon, K. Liebert, A. Siemion, J. Bomba, A. Sobczyk, W. Knap, D. Coquillet, J. Suszek, M. Sypek, *J. Infrared Millim. Terahertz Waves* 38, 347 (2017)
19. L. Kelian, H. Youli, S. Weifan, *Opt Commun* 339, 53 (2015)
20. M. Hashemi, A. Moazami, M. Naserpour, Z. J. Zapata-Rodriguez, *Opt Commun* 393, 77 (2017)
21. L. R. Rayleigh, *Opt Eng* 5, (1873)
22. J. Suszek, P. Zagrajek, M. Sypek Patent submission PL P.429535
23. M. Sypek, *Opt Commun* 116, 43 (1995).
24. Z. Jaroszewicz, A. Kolodziejczyk, M. Sypek, C. Gomez-Reino, *J Mod Opt* 43, 617 (1996)

Publisher's Note Springer Nature remains neutral with regard to jurisdictional claims in published maps and institutional affiliations.